

We are IntechOpen, the world's leading publisher of Open Access books Built by scientists, for scientists

5,600

Open access books available

137,000

International authors and editors

170M

Downloads

Our authors are among the

154

Countries delivered to

TOP 1%

most cited scientists

12.2%

Contributors from top 500 universities



WEB OF SCIENCE™

Selection of our books indexed in the Book Citation Index
in Web of Science™ Core Collection (BKCI)

Interested in publishing with us?
Contact book.department@intechopen.com

Numbers displayed above are based on latest data collected.
For more information visit www.intechopen.com



Chapter

New Ethylenediamine Crosslinked 2D-Cellulose Adsorbent for Nanoencapsulation Removal of Pb (II) and Cu (II) Heavy Metal Ions: Synthesis, Characterization Application, and RSM-Modeling

Issam Jilal, Soufian El Barkany, Zahra Bahari,

Youssef El Ouardi, Mohamed Loutou, Hassan Amhamdi,

Mohamed Abou-Salama, Amin Salhi,

Abderrahmane El Idrissi and Katri Laatikainen

Abstract

The main objective of the present work is to elaborate on a new eco-friendly and efficient adsorbent designated for aquatic micropollutants removal. However, the synthesis of the Ethylenediamine Crosslinked 2D-Cellulose green adsorbent was carried out successfully, by partial grafting of benzyl entities onto hydroxyl groups of HEC, and crosslinking with ethylenediamine ED. Further, the new ethylenediamine crosslinked 2D-Cellulose was used as a biosorbent for nanoencapsulation removal of copper and lead heavy metal ions from aqueous solutions. The proposal chemical structures of unmodified and modified materials were confirmed using FTIR, XRD, TGA, and SEM-EDX analysis. Furthermore, many parameters of the optimization for Pb (II) and Cu (II) in terms of removal efficiency including pH, adsorbent amount, and contact time were optimized by response surface methodology with a Box-Behnken design. Based on the desirability optimization with three factors, the maximal removal was 99.52% and 97.5% for Pb(II) and Cu (II), respectively and was obtained at pH = 5.94, 22.2 mg as the optimal adsorbent amount, and 21.53 min as contact time.

Keywords: Cellulose, Ethylenediamine, Adsorption, Lead, Copper, Nanoencapsulation

1. Introduction

In the last few decades, the fast development of industrialization and urbanization caused a tremendous and exponential increase in the human population, where

the avoidance of the quality deterioration of water, air, and soil becomes the priority [1]. However, the pollution of aquatic environments by industrial effluents, in particular, water pollution by heavy metals, is the most serious problem due to their non-biodegradable properties, their persistence in the environmental media [2–6], toxicity to human health and ecosystems [7, 8]. Currently, the elimination of metal ions remains a major issue for environmental sustainability, where the greatest source of heavy metals contamination of wastewater is directly linked to anthropic activities, in particular industrial (textiles, rubber, leather, paper, plastic, coal, food, petrochemicals, etc.), agricultural (pesticides, forestry, etc.), pharmaceutical and hydrometallurgical activities [9–11]. Lead (Pb) is considered one of the main pollutants present in different components of the biosphere, where it accumulates through trophic chains or water intake [12]. In addition, Pb (II) ions are able, even at low concentrations, to causing severe central nervous system damage, kidney and immune system dysfunction in human beings, especially for children [8, 13–16]. Given its exceptional electrochemical aspect, copper occupies a prominent place in the international economy, where paving a large industrial area (energy, information, telecommunication, electronics, etc.), which is considered the second strategic raw material, in China, after oil [17, 18].

At the light of this, to decontaminate the industrial effluents from heavy metal ions, the efforts integrate the different separation techniques such as chemical precipitation [19, 20], membrane filtration [21, 22], flocculation and chemical coagulation [23, 24], biological treatment [25], ion exchange [26, 27], photocatalytic degradation [28], advanced oxidation [29], nanofiltration [30–32], and adsorption [33–38]. However, the adsorption process remains the most interesting and attractive technique due to its simplicity, ease of handling, high efficiency, ability to remove a large amount of organic and inorganic pollutants, and availability [39–42]. Faced with environmental constraints, the modern industrial policy requires well-defined qualities for basic adsorbent materials such as stability, retention capacity, low cost, biodegradability, etc. [43]. In this regard, cellulose, the most abundant, renewable, non-toxic, biodegradable, biocompatible, inexpensive, and environmentally friendly biopolymer in the world [44–48] has attracted increasing attention meeting ecological criteria [35, 49–51]. However, native cellulose showed a low adsorption capacity that indicating a low surface charge density. Thus, to improve its reactivity, it is necessary to reduce structurally related recalcitrance, where the exceptional chemical structure of cellulose, in particular the hydrogen bond type interactions at the supramolecular level, prevents its dissolution in almost all conventional solvents [52]. Another way to introduce new functionalities is to use cellulosic derivatives with more reactive accessibility. A good example of these derivatives is hydroxyethylcellulose (HEC), which makes it possible to obtain good solubility in an alkaline medium and water [53]. In addition, the reactivity of HEC is greater than that of cellulose because the density of the primary alcohol entities has increased [33], which gives the possibility of good control of the degree of substitution (DS), in particular for Williamson etherification of HEC grafted benzyl entities, where solubility has been successfully achieved and controlled in common solvents [54].

In this work, HEC was used as a water-soluble derivative of cellulose, where it was partially hydrophobized by introducing benzyl functionalities to decrease the average functionality of the reaction system, to avoid the 3D crosslinking in the following stage of the reaction, which ensures good accessibility of the pollutant load during the adsorption process, this ecological synthesis showed, in our previous article, that the degree of substitution does not exceed unity [33, 53–55]. Then, the benzyloxyethylcellulose (BEC) polymer chains were crosslinked using ethylenediamine (ED) as a crosslinking agent and as a bidentate metal ion chelator,

especially for the removal of Pb (II) or Cd (II) [56–64]. Structural analyzes showed good agreement with the proposed structure of the new green adsorbent (BEC-ED). X-ray diffraction patterns and SEM confirmed the emergence of a new structural order of BEC-ED at the crystalline and morphological levels. However, the elemental surface profile of BEC-ED has been proven based on the EDS spectra. The effect of crosslinking on the ability to remove heavy metals from aquatic environments was studied as a function of physicochemical parameters (pH, nature of ions, contact time, initial concentration, etc.), which are optimized using the response surface methodology with the *Box–Behnken* design. To our knowledge, based on a review of the literature, the new green BEC-ED has never been described previously.

2. Materials and methods

2.1 Materials

HEC (DS \sim 1.5) of 95% purity was purchased from HIMEDIA and it was purified by the dissolution-precipitation method in water-acetone solvents. Tetrahydrofuran (THF), ethylenediamine ED, thionyl chloride (SOCl₂), DMSO, hydrochloric acid (HCl) 37%, and triethylamine (Et)₃N were used as received from Sigma-Aldrich. Sodium hydroxide (NaOH) and Benzyl bromide were purchased from Merck. All other chemicals are analytical grade and were used as received without any further purification.

2.2 Methods

Fourier Transform Infrared spectroscopy (FTIR) spectra of the HEC, BEC, and BEC-ED samples were recorded on Shimadzu FTIR-8400S spectrometer using finely ground KBr pellets with 2% of the sample at a resolution of 2 cm⁻¹. The measurements were performed over from 4000 to 400 cm⁻¹, and averages of 40 scans were taken for each sample. The morphological SEM images of HEC, BEC, and BEC-ED were investigated using scanning electron microscopy (TESCAN VEGA 3 LM), with an accelerating voltage of 10 kV. Energy-dispersive X-ray spectra (EDS) were recorded to divulge the elemental profile presenting on unmodified and modified polymer surfaces. The sample crystal orders were evaluated using the X-ray diffraction technique and were obtained from EQUINOX 2000an X-ray Diffractometer, using copper radiation CuK α (λ = 1.5418 Å), at an accelerating voltage of 40 kV and an operating current of 30 mA. All patterns are recorded in the range of 2θ (5°–35°). 0.25 g of each sample was pressed under 50 MPa to form pellets having an average of 25 mm in diameter. The thermal behavior of each sample was carried out on simultaneous DTA-TG Shimadzu DTG-60 apparatus. The amounts of the samples were between 8 and 12 mg and the interval of the temperature measurement was between room temperature and 600°C with a heating rate of 10°C min⁻¹ under nitrogen flow. For all experiments, lead and copper ions concentrations were obtained by inductively coupled plasma-atomic emission spectroscopy on an ICP-AES (Iris Intrepid IIXDL ICP-AES).

2.2.1 Preparation of BEC-ED

BEC was prepared according to the method described in our previous paper [54]. First, the crosslinking of BEC is carried out by passing through the chlorination of the free OH groups, as an intermediate step. Where, to 1 g (2.6 mmol) of the BEC dissolved in the minimum of DMSO, 0.38 ml (2.7 mmol) of (Et)₃N and

0.40 ml (5.5 mmol) of Thionyl chloride SOCl_2 were added dropwise. The reaction mixture was heated at 70°C for 2 h under stirring. The product is precipitated in water, filtered under vacuum, and then treated with 2% ammonia solution to neutral pH. Finally, the sample was washed frequently with water, filtered, and dried at 70°C . Ethylenediamine crosslinked BEC (BEC-ED) was carried out in THF at reflux for 4 h, where 1 g of BEC-Cl was reacted with ED in large excess (6 ml) using TEA as a capturing agent of HCl released. At the end of the reaction, the resulting product (white powder) was isolated by filtration under vacuum and frequently laved by distilled water to remove the ammonium salt and ED excels.

3. Results and discussions

3.1 Synthesis and characterization

BEC-ED synthesis was performed after HEC hydrophobization (partial benzylation) to decrease the rate of crosslinking in bio-adsorbent. In addition, crosslinking was performed with ED to study the effect of graft grouping on the ability to remove heavy metals from aquatic environments. The originality of this work is summed up in the fact that this type of product has never been described previously in the literature. The reaction scheme for the synthesis of BEC-ED, as a novel heavy metal adsorbent in aquatic media, is shown in **Figure 1**. The

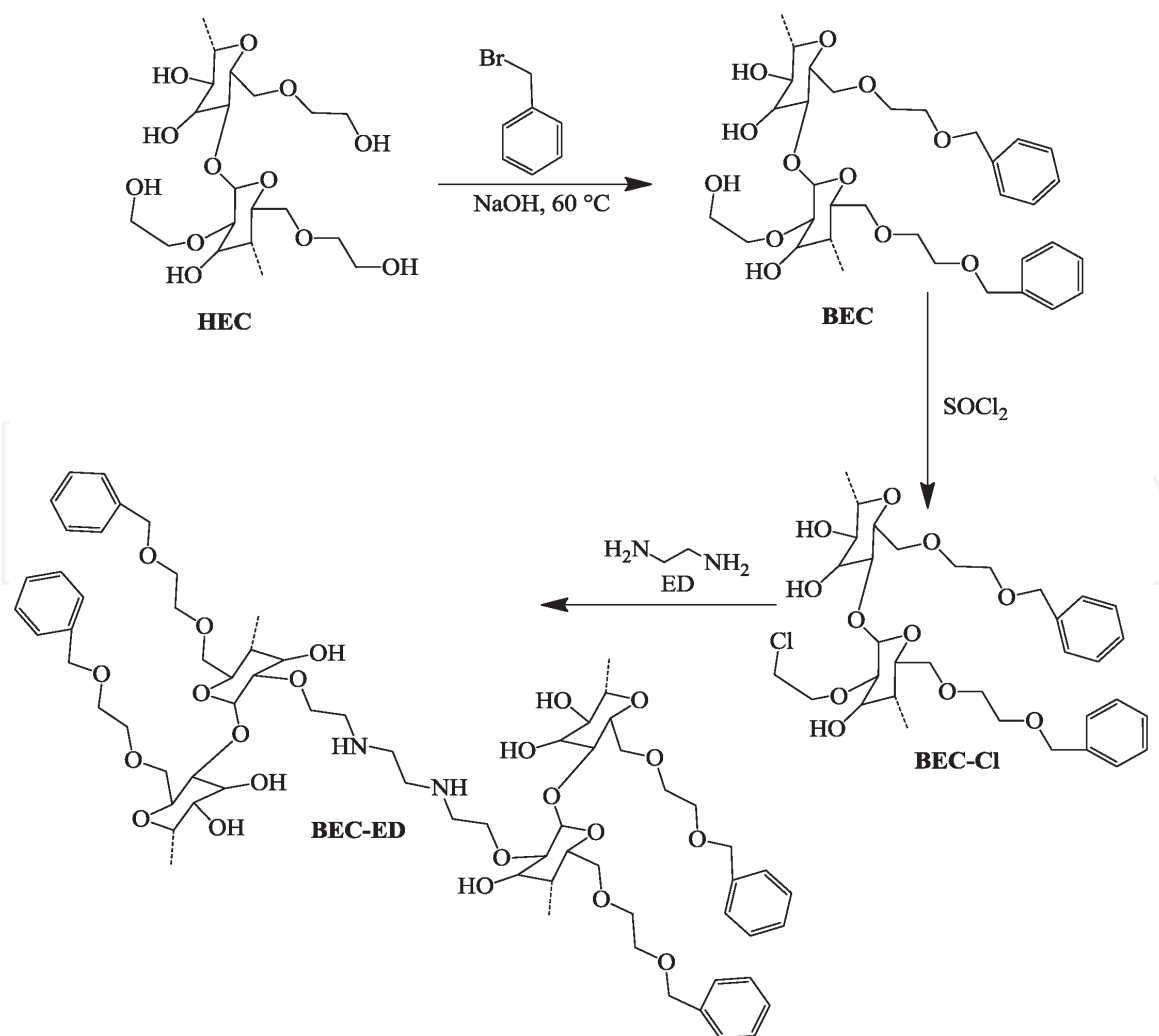


Figure 1.
Reaction scheme of the preparation of BEC-ED.

crosslinking of BEC is carried out through the chlorination of the free OH groups, as an intermediate step, and then crosslinked by the ED in the THF using Triethylamine as the capturing agent of the released HCl to avoid the degradation of the cellulose chain under the effect of acid. However, the apparition of the white powder during the reaction indicating that the reaction of the crosslinking has been carried out successfully.

3.1.1 Structural analysis (FTIR)

FTIR spectra of HEC, BEC, BEC-Cl, and BEC-ED are given in **Figure 2**. The FTIR of unmodified HEC spectrum showed infrared absorption bands spotted at 1062, 1408, 1458, 2873, 2927, and 3412 cm^{-1} . The absorption band at 3412 cm^{-1} is attributed to O–H stretching vibration [65], and a medium absorption band located in the range of 2927 and 2873 cm^{-1} corresponds to the C–H stretching vibration [66]. Moreover, the characteristic bands situated around 1408 and 1458 cm^{-1} are attributed to C–H symmetric bending vibration in –CHOH and O–H plane deformation of a primary alcohol, respectively [55]. The absorption band of b-(1,4)

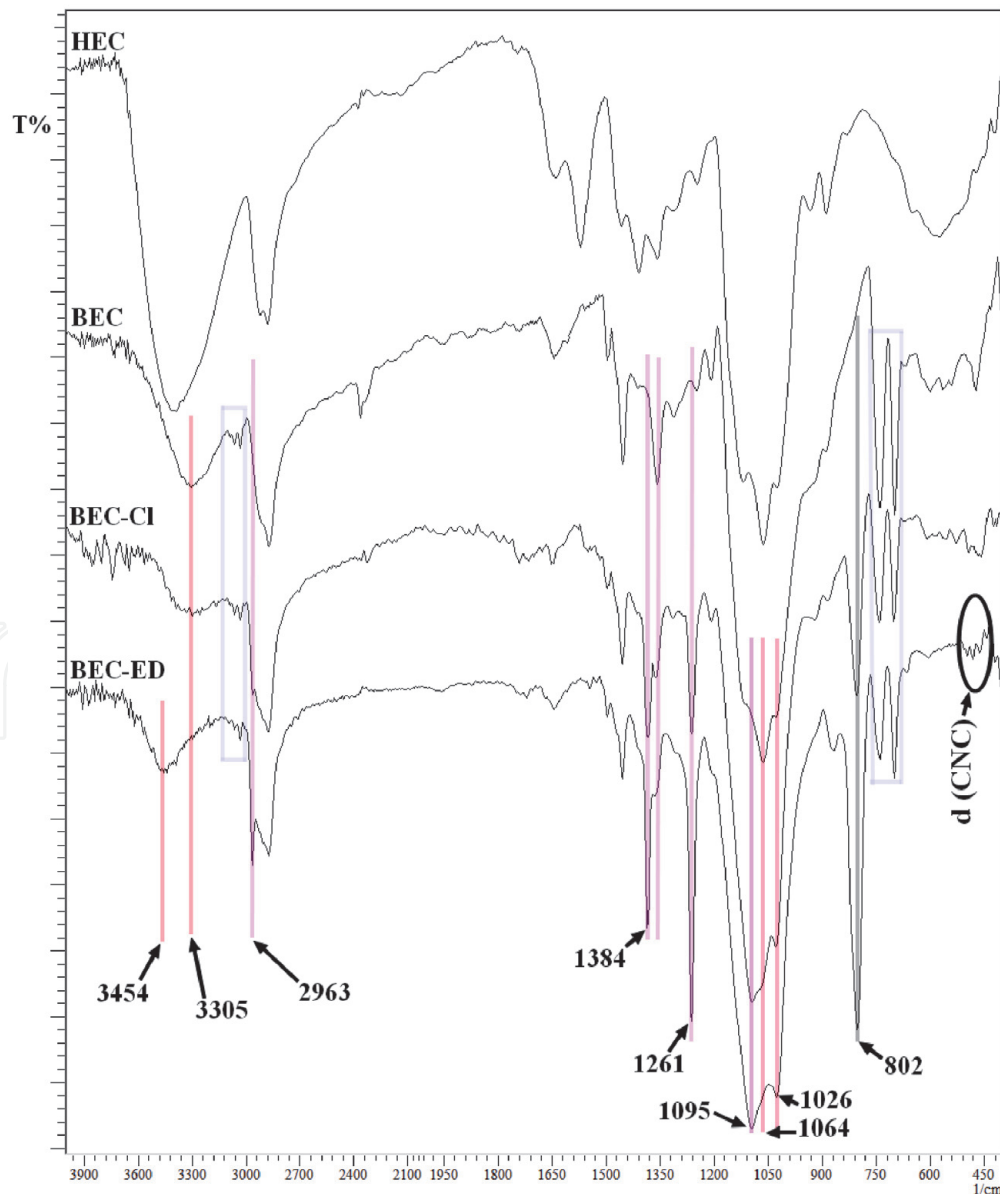


Figure 2.
The FTIR spectra of HEC, BEC, BEC-Cl and BEC-ED.

glycoside linkage was observed at 887 cm^{-1} [67], and that of C–O–C stretching vibration in the glucopyranose at 1062 cm^{-1} [68]. The absorption band at 1120 cm^{-1} corresponds to the C–O asymmetric vibration [67]. It can be seen, in **Figure 2**, that the modification of HEC by the benzyl group is apparent with a decrease in the intensity of the peak at 3347 cm^{-1} indicating a benzyl substitution of OH groups [69]. Indeed, the aromatic characteristic band elongations (=C–H) are situated between 3090 and 3033 cm^{-1} [70] and the aromatic C=Csp² elongation vibrations are located at 1454 cm^{-1} [71]. In addition, the appearance of new absorption bands corresponding to the angular deformation (out of plane) of the monosubstituted aromatic C–H at around 740 cm^{-1} [72], and the C=C aromatic angular deformation, situated at 698 cm^{-1} , is a strong indication of the benzyl group incorporation on the HEC polymeric structure.

The comparison of FTIR spectra of unmodified BEC and chlorinated BEC (BEC-Cl) shows that the chlorination of BEC was carried out with success. Indeed, the new absorption band at 802 cm^{-1} , attributed to the stretching of the carbon-chlorine bond C–Cl, is a strong indication that confirming the chlorination reaction. In addition, the decrease in band intensity at 3305 cm^{-1} is due to the substitution of the hydroxyl group by chlorine, which confirms the success of the reaction [73, 74]. After BEC crosslinking, the appearance of the characteristic –NH– absorption band between 3305 cm^{-1} and 3454 cm^{-1} designates the incorporation of amino entities into the BEC structure. The increase in the density of –CH₂– groups in the cellulosic skeleton is noticed through the increase in the intensity of the absorption band corresponding to the stretching vibrations of the methylene (–CH₂) groups at 2963 cm^{-1} . Furthermore, the ED crosslinking BEC is confirmed by the appearance of the different characteristic bands of the amino groups, which are located at 1095 cm^{-1} and 1590 cm^{-1} corresponding to the NH and CN stretching vibrations, respectively [75]. Thus, the intense peak attributed to the out-of-plane strain of NH at 802 cm^{-1} is very remarkable [75]. Also, the reduction in the intensity of the CO alcohol characteristic band around 1200 cm^{-1} is a strong indication of the substitution of OH by NH of ED [76–78].

3.1.2 Scanning electron microscopy, energy-dispersive x-ray (SEM-EDS) spectroscopy

Figure 3 shows SEM images of HEC, BEC, and BEC-ED. The resulted SEM images obtained for BEC showed homogenous, continuous, and microporous morphology, where pores diameter was estimated about (1–2) μm , which is radically different from the HEC aggregation aspect and lamellar BEC-ED morphologies. Yet, the morphological character of BEC allows it to be considered as a good candidate for microporous adsorbent/membranes applications. However, the EDS spectra of HEC and BEC showed a very significant increase in the C/O ratio, which indicates that the benzyl entities are grafted successfully. The evidence of BEC crosslinking by ED is shown by the EDS spectrum corresponding to BEC-ED, where the peak corresponding to nitrogen is very noticeable. In addition, BEC-ED SEM images showed a Nanoscale laminated appearance, including a lamellar structure that occurs through hydrophobic interactions. Based on BEC-ED morphology results, a supramolecular structure is proposed and schematically illustrated in **Figure 4**.

3.1.3 X-ray diffraction (XRD)

Figure 5 shows the X-ray diffractograms of HEC, BEC, and modified BEC (BEC-ED) in the range of $2\theta = 00^\circ$ to 37° . According to the diffractograms of the two polymers (HEC and BEC), the benzylation of HEC has practically no effect on the crystal behavior of HEC, except for a small shift of the maximum diffraction

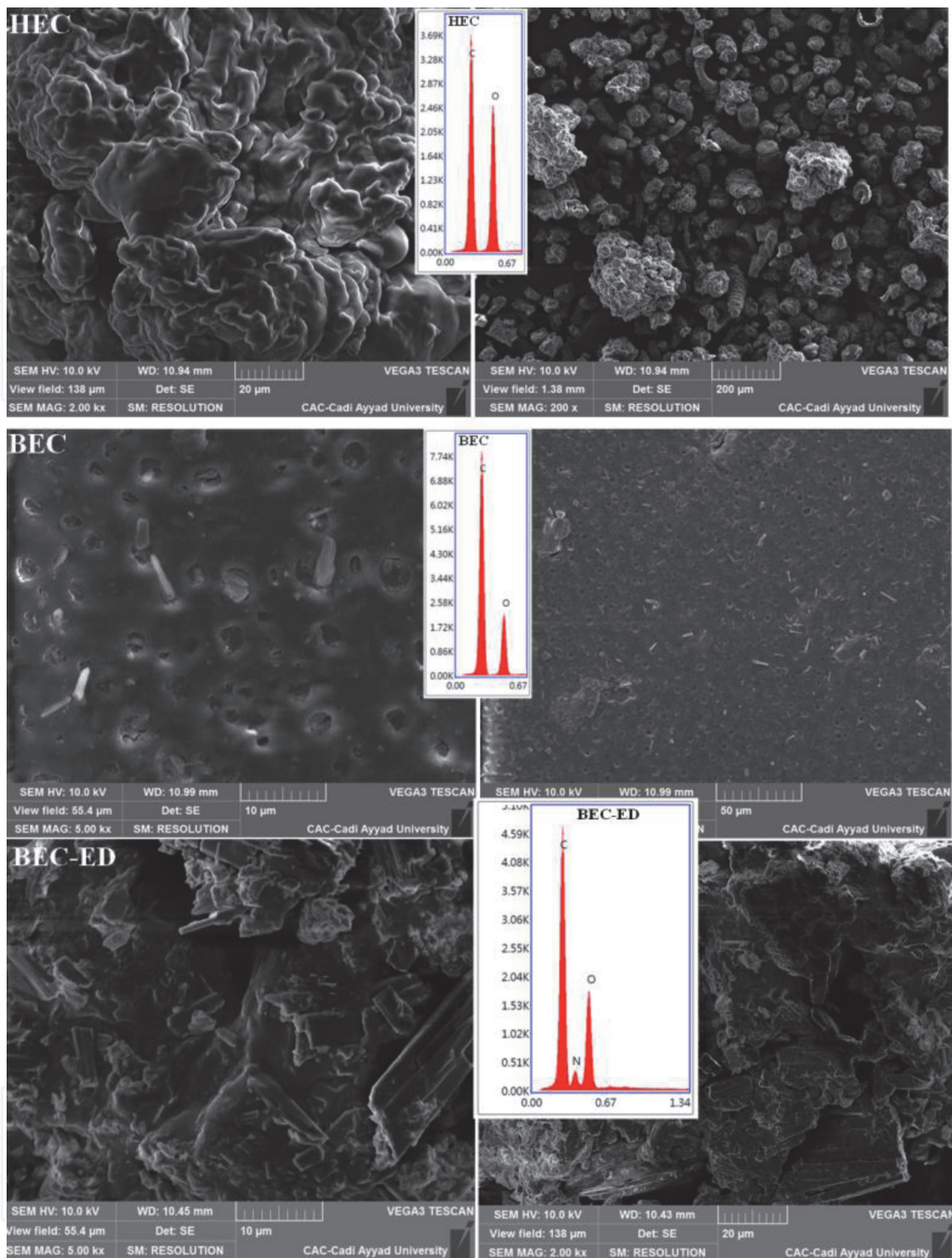


Figure 3.
 SEM images and EDS spectra of HEC, BEC and BEC-ED.

peak towards the low values of HEC, 2θ of 21.25° for HEC and 20.80° for BEC, but the predominance of the amorphous character is always considered. Though, the small decrease in 2θ , at this region, can be explained by the increase in the supra-molecular distance, between macromolecular chains, resulting from the insertion of benzyl entities. On the other hand, the diffractogram of the modified BEC sample (BEC-ED) showed, comparing to BEC, very remarkable and significant changes. Indeed, the crosslinking reaction of BEC generated a new crystalline order characterized by the apparition of a new peak towards $2\theta = 12.50^\circ$, which corresponds to a lattice distance of 07.07 \AA (Figure 5). The presence of a large domain with a

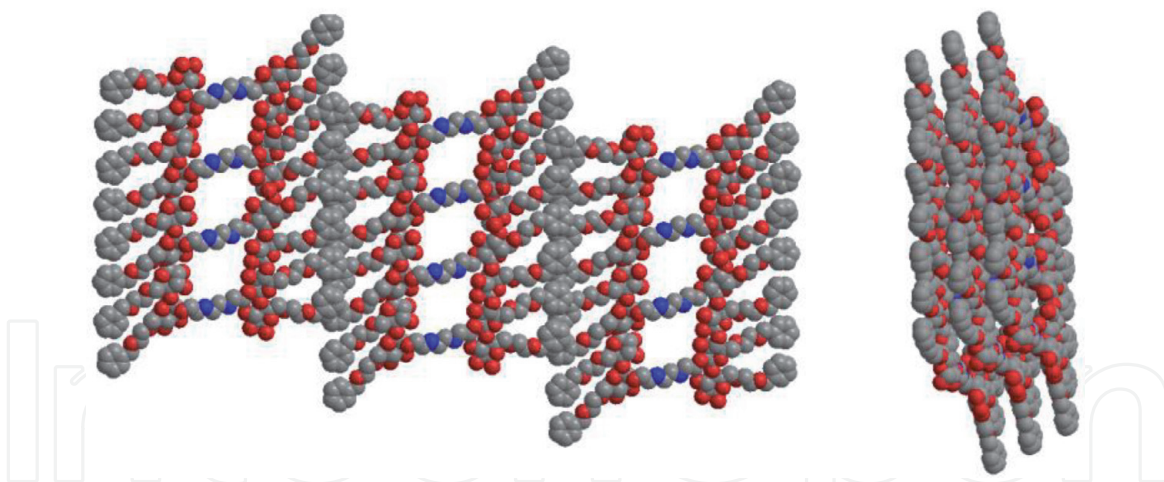


Figure 4.
Supramolecular lamellar structure of BEC-ED.

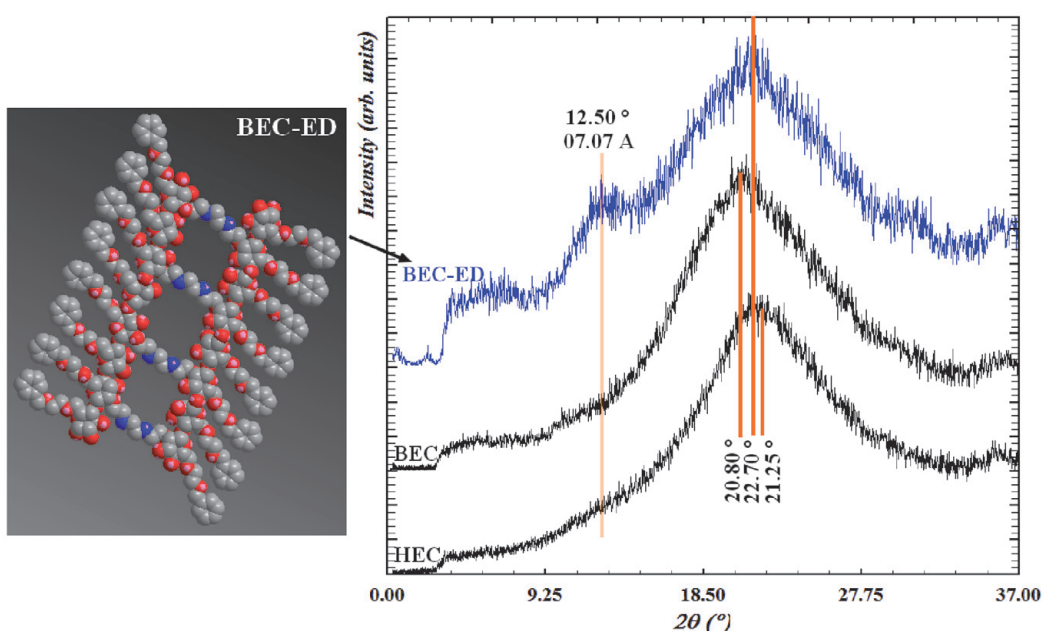


Figure 5.
Supramolecular structure of BEC-ED and the XRD diffractograms of HEC, BEC and BEC-ED.

maximum at $2\theta = 22.7^\circ$, on the BEC-ED diffractogram, reveals its amorphous character. Therefore, a semi-crystalline appearance of BEC-ED can be suggested.

3.1.4 Thermogravimetric analysis (TGA)

Thermogravimetric makes it possible to follow, as a function of temperature, the weight loss evolution of each sample, mainly caused by dehydration or/and by the decomposition of the organic matter it contains. The thermal stability of BEC-ED comparing to BEC is studied basing on the TGA thermograms shown in **Figure 6**. The thermal behavior of BEC shows two stages of thermal decomposition, the first one is observed between 35 and 250°C attributed to the solvents and adsorbed water vaporization [79]. The strong weight loss (70%) corresponds to the degradation of the grafted entities and the cellulose backbone is observed in the temperature range of 250–600°C. For BEC-ED, no thermal event was observed below 250°C, indicating the absence of traces of solvents. The thermal decomposition of BEC-ED is noticed from 250°C up to 450°C with a mass loss of 90%. In addition, a low degradation of the thermal stability of BEC-ED compared to BEC has been noted,

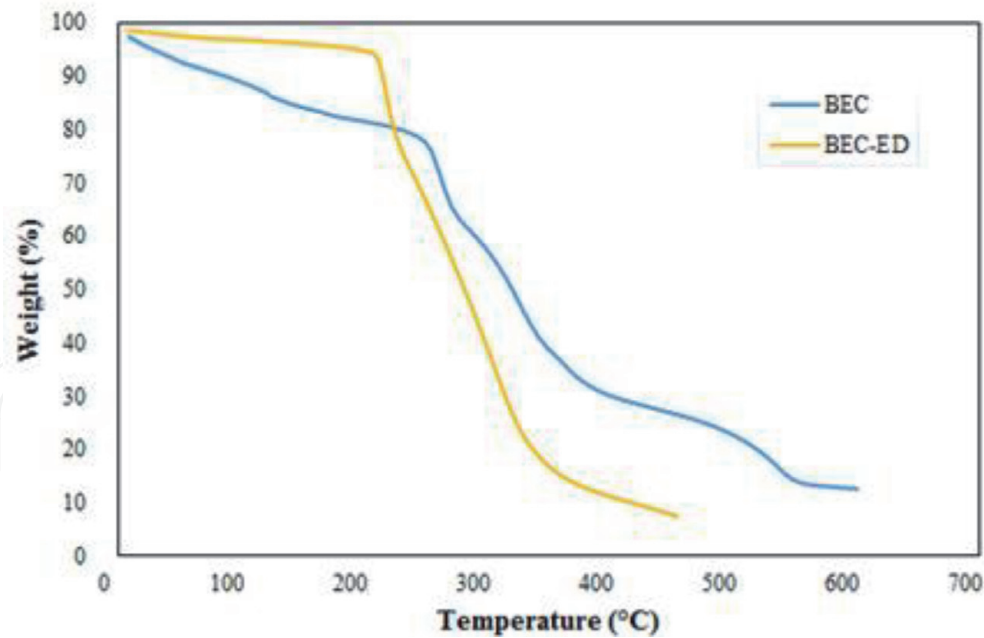


Figure 6.
 TGA thermogram profiles of BEC and BEC-ED.

Variables	Factors	Unit	Level 1 (-1)	Level 2 (0)	Level 3 (1)
X_1	Ph	—	4.5	6	7.5
X_2	Adsorbent amount	mg	10	20	30
X_3	Contact time	min	5	17.5	30

Table 1.
 Coded and actual variables and their levels.

and this is possibly due to the decrease of hydrogen interaction density and their replacement by hydrophobic interactions, and the supramolecular separation of the polymer chains caused by grafted ethylenediamine (ED).

3.2 Response surface methodology (RSM) modeling procedure

In the current work, is focused on 3-level Box–Behnken design (BBD) in response surface methodology for seeking the optimal conditions for the removal efficiency of Cu(II) and Pb(II) onto BEC-ED. The three variables affecting the current process are pH at 4.5, 6.0, and 7.5, contact time at 5, 17.5, and 30 min, and adsorbent amount at 10, 20 and 30 mg. The complete design consisted of three different levels (-1, 0, and +1) and 3-variable (pH— X_1 , Adsorbent amount — X_2 , and contact time — X_3). The layout of the factorial design is shown in **Table 1**. A total of 17 experiments were used in this study to evaluate the effects of the three input variables on Pb(II) and Cu(II) removal efficiency. The full picture of experiments with their responses (Pb(II) and Cu(II) removals) are tabulated in **Tables 2** and **3**, respectively.

The analysis of variance (ANOVA) was applied to the experimental runs, and then the results of the Box–Behnken design table are calculated and fitted by a suitable polynomial equation. According to the model's evaluation in **Tables 4** and **5**, which focuses on maximum R^2 , predicted R^2 , and adjusted R^2 , the quadratic polynomial (Eq. (1)) model was chosen and well-fitted for all three independent parameters and responses (Cu(II) and Pb(II) removal efficiency).

	Factor 1	Factor 2	Factor 3	Response 1	Response 2
Run	X ₁ :pH	X ₂ :Adsorbent amount	X ₃ :Contact time	Pb removal	Cu removal
		Mg	min	%	%
1	0	0	0	95.64	91.21
2	1	-1	0	40.27	43.24
3	-1	1	0	61.85	57.57
4	0	0	0	96.41	93.32
5	-1	0	-1	43.53	45.92
6	-1	-1	0	42.85	39.84
7	0	0	0	96.23	94.78
8	0	1	-1	69.08	73.12
9	1	0	-1	42.82	51.48
10	0	1	1	92.42	91.37
11	1	1	0	62.32	61.76
12	0	-1	1	68.34	62.28
13	-1	0	1	67.24	68.84
14	0	0	0	94.86	94.81
15	0	-1	-1	47.17	49.53
16	0	0	0	93.81	91.76
17	1	0	1	64.87	65.67

Table 2.

The BBD matrix design with three independent factors and the corresponding experimental results.

Source	Sum of Squares	df	Mean Square	F-value	p-value	
Model	7460.88	9	828.99	730.00	< 0.0001	Significant
A-pH	3.37	1	3.37	2.96	0.1288	
B-Amount	947.00	1	947.00	833.92	< 0.0001	
C-Time	1018.58	1	1018.58	896.96	< 0.0001	
AB	2.33	1	2.33	2.05	0.1955	
AC	0.6889	1	0.6889	0.6066	0.4616	
BC	1.18	1	1.18	1.04	0.3425	
A ²	3566.13	1	3566.13	3140.31	< 0.0001	
B ²	880.99	1	880.99	775.80	< 0.0001	
C ²	573.67	1	573.67	505.17	< 0.0001	
Residual	7.95	7	1.14			
Lack of Fit	3.36	3	1.12	0.9779	0.4866	Not significant
Pure Error	4.59	4	1.15			
Cor Total	7468.83	16				

Table 3.

ANOVA analyses of the quadratic model and determination coefficients for Pb(II) adsorption efficiency.

Source	Std. Dev.	R ²	Adjusted R ²	Predicted R ²	PRESS	
Linear	20.57	0.2636	0.0937	-0.1046	8249.92	
2FI	23.44	0.2642	-0.1773	-0.9645	14672.20	
Quadratic	1.07	0.9989	0.9976	0.9918	60.98	Suggested
Cubic	1.07	0.9994	0.9975		*	Aliased

*Case(s) with leverage of 1.0000: PRESS statistic not defined.

Table 4.
 Model summary statistics Pb(II).

Source	Std. Dev.	R ²	Adjusted R ²	Predicted R ²	PRESS	
Linear	19.32	0.2466	0.0728	-0.1445	7370.22	
2FI	21.97	0.2508	-0.1987	-1.0514	13210.51	
Quadratic	2.73	0.9919	0.9815	0.8955	672.91	Suggested
Cubic	1.67	0.9983	0.9931		*	Aliased

*Case(s) with leverage of 1.0000: PRESS statistic not defined.

Table 5.
 Model summary statistics Cu(II).

Therefore, the predictive polynomial quadratic response model can be described as the following equation (Eq. (1)) [80]:

$$Y = \beta_0 + \sum_{i=1}^n \beta_i X_i + \sum_{i=1}^n \beta_{ii} X_i^2 + \sum_{i=1}^n \sum_{i>1}^n \beta_{ij} X_i X_j \quad (1)$$

Where Y is the predicted response, β_0 and β_i are the intercept coefficient, and the linear coefficient respectively, β_{ii} and β_{ij} are the quadratic and the interaction coefficients, respectively, while X_i and X_j represent the coded values of the independent variables.

An ANOVA analysis for Cu (II) and Pb (II) removals was performed, and the results are presented in **Tables 3** and **6**, respectively. According to ANOVA analysis, the results obtained showed that the F and P-values less than 1000 and 0.0500, respectively. This confirmed that the model terms are significant. While **Lack of Fit F-value** in the ANOVA tables introduces an insignificant error with regard to the pure error. The response for Cu(II) and Pb(II) removal efficiency was determined with real factors by the following expressions (Eqs. (2) and (3)):

$$\begin{aligned} Pb(II) \text{ Removal} = & -480.655 + 154.152 * pH + 6.49305 * Amount + 3.56334 * Time \\ & + 0.0508333 * pH * Amount + -0.0221333 * pH * Time + 0.00434 * Amount * Time \\ & + -12.9344 * pH^2 + -0.14465 * Adsorbent amount^2 + -0.074704 * Time^2 \end{aligned} \quad (2)$$

$$\begin{aligned} Cu(II) \text{ Removal} = & -462.971 + 146.053 * pH + 7.18408 * Amount + 3.02441 * Time \\ & + 0.00816667 * pH * Amount + -0.1164 * pH * Time + 0.011 * Amount * Time + \\ & -11.9436 * pH^2 + -0.157755 * Amount^2 + -0.0532832 * Time^2 \end{aligned} \quad (3)$$

Statistical diagnostics test is an excellent and effective tool for confirming the model presented. These diagnostic plots are given in **Figure 7**. By classifying the

Source	Sum of Squares	df	Mean Square	F-value	p-value	
Model	6387.74	9	709.75	95.35	< 0.0001	Significant
A-pH	13.21	1	13.21	1.77	0.2245	
B-Amount	995.25	1	995.25	133.71	< 0.0001	
C-Time	579.87	1	579.87	77.90	< 0.0001	
AB	0.0600	1	0.0600	0.0081	0.9310	
AC	19.05	1	19.05	2.56	0.1536	
BC	7.56	1	7.56	1.02	0.3470	
A ²	3040.67	1	3040.67	408.51	< 0.0001	
B ²	1047.86	1	1047.86	140.78	< 0.0001	
C ²	291.85	1	291.85	39.21	0.0004	
Residual	52.10	7	7.44			
Lack of Fit	40.97	3	13.66	4.91	0.0792	Not significant
Pure Error	11.13	4	2.78			
Cor Total	6439.84	16				

Table 6. ANOVA analyses of the quadratic model and determination coefficients for Cu(II) adsorption efficiency.

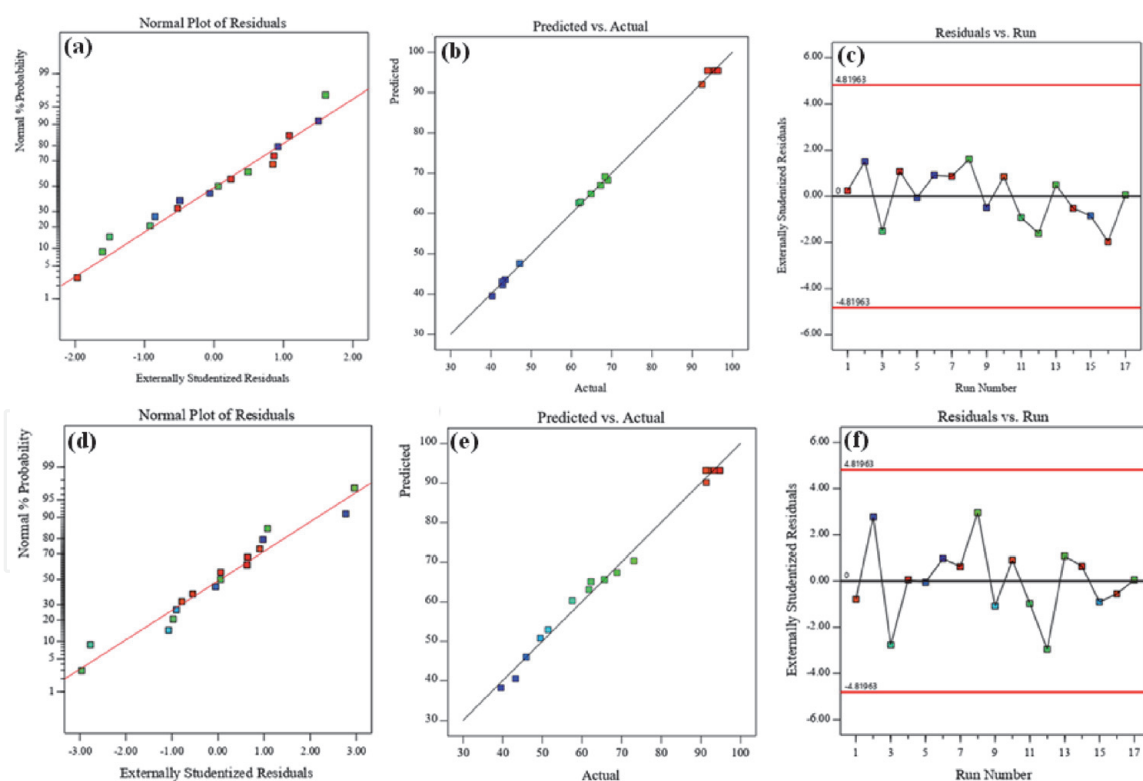


Figure 7. Diagnostic plots for adsorption of Pb(II): Probability plot for the studentized residuals (a), comparison between actual and predicted values (b), plot of the externally studentized residuals vs. experimental run number (c), diagnostic plots for adsorption of Cu(II): Probability plot for the studentized residuals (d), comparison between actual and predicted values (e), plot of the externally studentized residuals vs. experimental run number (f).

proportion of normal probability in terms of residuals, it can be observed that the datum-points are approximately straight-line (**Figure 7a** and **d**). Into the other diagnostic plots, the actual responses were compared to their residuals based on

predicted responses, suggesting that the quadratic model was required to predict removal efficiency in the experimental parameters (**Figure 7b** and **d**). In addition, as shown in the plot (**Figure 7c** and **f**) the data showed a good homogeneity. In **Figure 7**, the dispersion of the residuals is dispersed randomly about ± 5 , confirming that the results are coherent with the model. In the other diagnostic plots, actual responses were compared to their residues based on predicted responses, implying that the quadratic model was necessary to predict removal efficiency in experimental parameters.

By employing the RSM method, the evaluated models (Eqs. (2) and (3)) are used to design the 3-D graphs and find the optimal conditions for Pb (II) and Cu(II) removal efficiency. It can be seen from **Figures 8** and **9** that the retention of Pb(II) and Cu(II) ions onto BEC-ED increases with increases of the pH solution. The removal efficiency reached a maximum of around 6. When the pH is higher than 6 or lower than 5 the adsorption decreased rapidly. This could be explained by that in the acidic environment, the active groups responsible for the adsorption process exist mainly in the NH_3^+ form, and they prevent the retention of Pb (II) and Cu(I) ions on the amino groups of BEC. When the pH increases from 2 to 5, the active sites of the chelator become in the form of free NH_2 amines, which facilitate chelation on Pb(II) [60]. In addition, at high pH, the formation of lead and copper hydroxides (**Figure 10**) limits their adsorption on the BEC-ED surface, and as shown in **Figures 8** and **9**, at high pHs, the removal efficiency of Pb(II) and Cu(II) ions is significantly diminished. Contact time was also examined and as given in **Figures 8** and **9**. The results of the retention of Pb(II) and Cu(II) onto BEC-ED revealed that the maximum adsorption equilibrium can be achieved rapidly around 16 min.

In conclusion, based on the desirability optimization with three factors, the best removal efficiency was 99.52% and 97.5% for Pb(II) and Cu(II), respectively and was obtained at pH: 5.94, adsorbent amount: 22.2 mg, and contact time: 21.53 min (**Figure 11**).

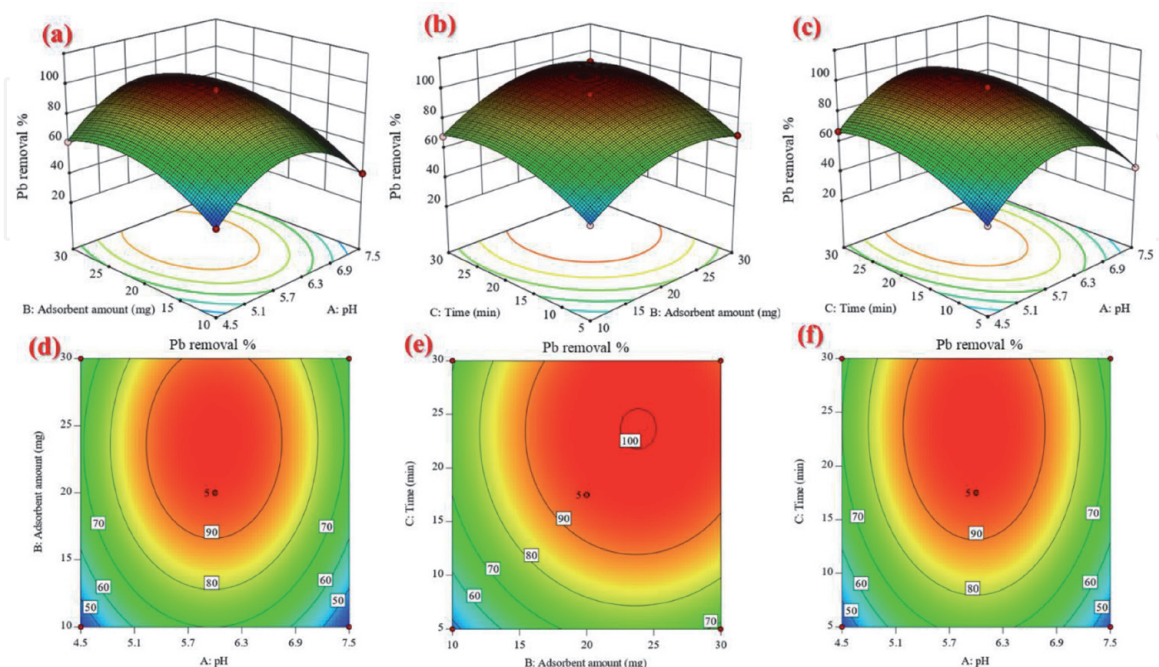


Figure 8. (a, b and c) 3D response surface plot and, (d, e and f) contour plot for the effect of factors on the Pb(II) removal efficiency.

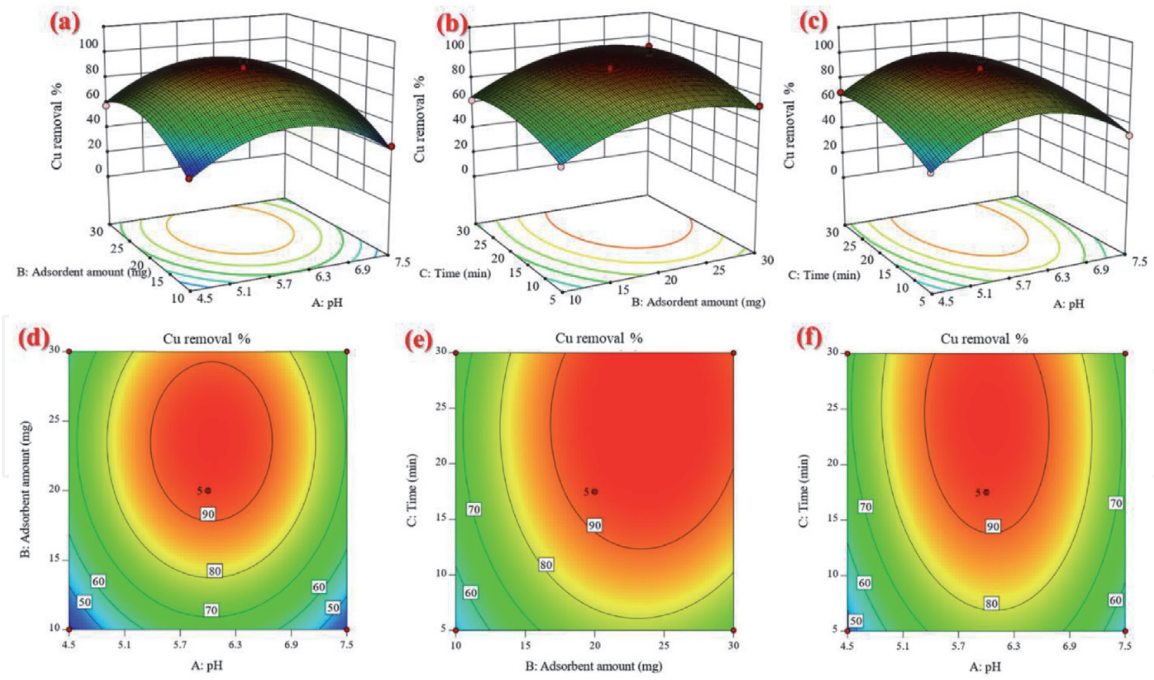


Figure 9. (a, b, and c) 3D response surface plot and, (d, e and f) contour plot for the effect of factors on the Cu(II) removal efficiency.

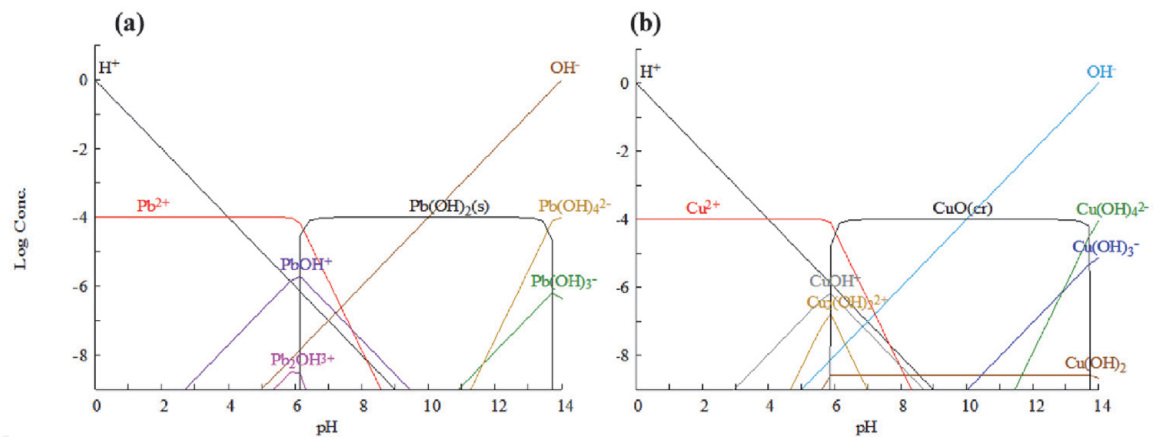


Figure 10. Speciation diagram of lead (a) and copper (b) as a function of pH in ultrapure water, determined by the hydra/medusa program [81].

3.3 Equilibrium isotherms

Adsorption isotherms for lead and copper were made by carrying out batch adsorption studies. Lead and copper adsorption was studied onto BEC-ED in a large concentration range (from 15 to 250 mg/L), to better model the retention mechanisms. The adsorption experiments were performed at room temperature by using a mass of adsorbent 22.2 mg with 50 mL of the aqueous solution, at pH 5.94 and contact time 21.53 min. The quantity of the lead and copper ions adsorbed onto the BEC-ED at equilibrium, q_e (mg/g), and the adsorption percentage was calculated by the following Equations [82]:

$$q_e = \frac{(C_0 - C_e)}{m} \times V \quad (4)$$

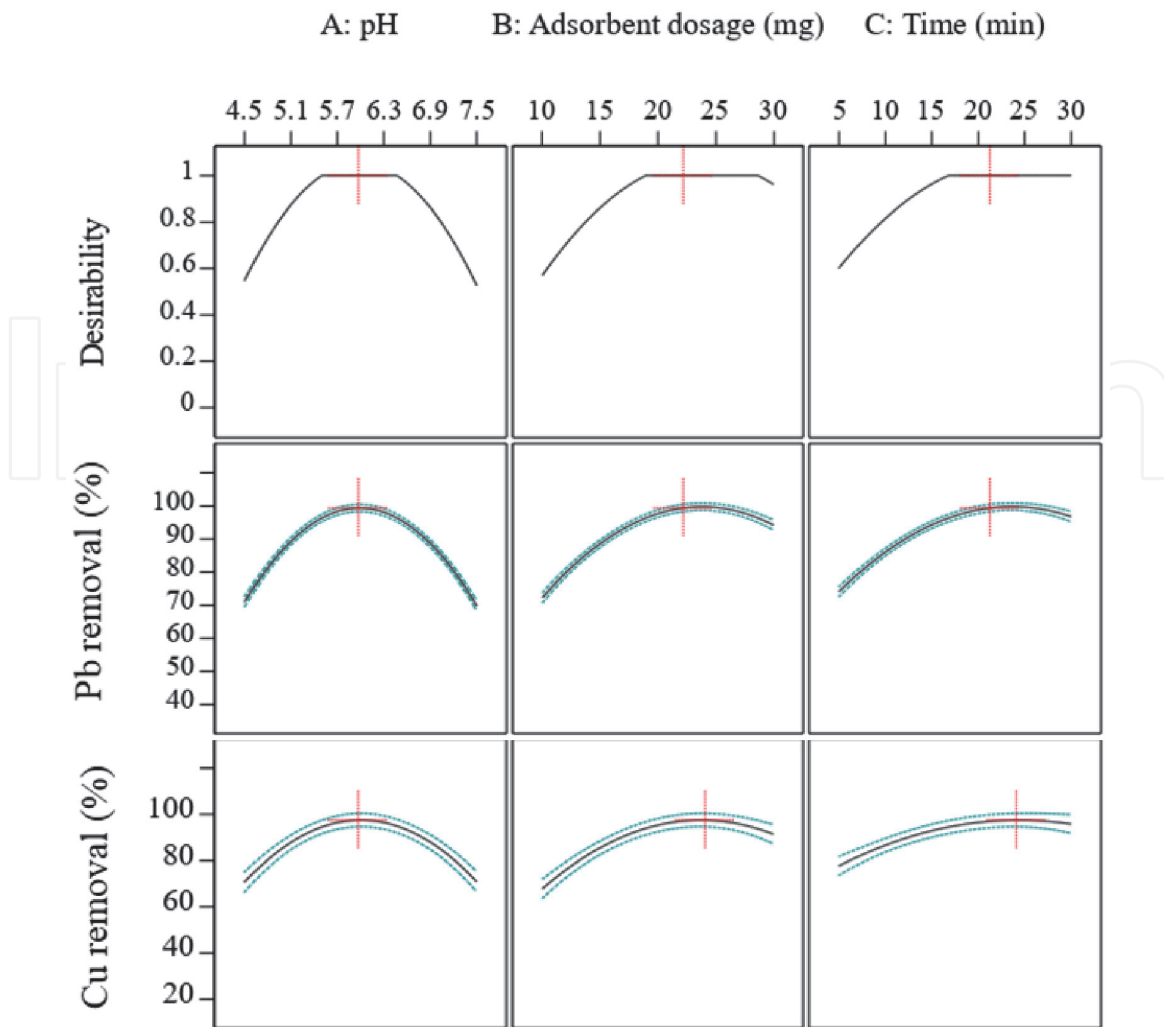


Figure 11. Desirability approach function optimization for Pb(II) and Cu(II) in terms of removal efficiency (%) and desirability.

$$\%Adsorption = \left(1 - \frac{C_e}{C_0}\right) \times 100 \quad (5)$$

Where, C_0 and C_e are the metal ion initial concentration and concentration at equilibrium (mg/L), respectively. V is the volume of solution (L) and m is the adsorbent amount (g).

The adsorption isotherms of Cu(II) and Pb(II) on BEC-ED were modeled using the Freundlich (Eq. (6)) [83] and Langmuir (Eq. (7)) [84] models equations:

$$q_e = K_F C_e^{1/n} \quad (6)$$

Where, n and K_F are Freundlich constants represent the heterogeneity index, and the adsorption coefficient, respectively.

$$q_e = \frac{q_m K_L C_e}{1 + K_L q_m} \quad (7)$$

Where, K_L (L/mg) and q_m (mg/g) are the Langmuir constant and the maximum adsorption capacity, respectively.

The equilibrium isotherm obtained for lead and copper adsorption on BEC-ED is shown in **Figure 12**. Lead adsorption was greater than that of copper 43.85 mg/g. This could be explained by the higher reactivity of lead than copper, which can have

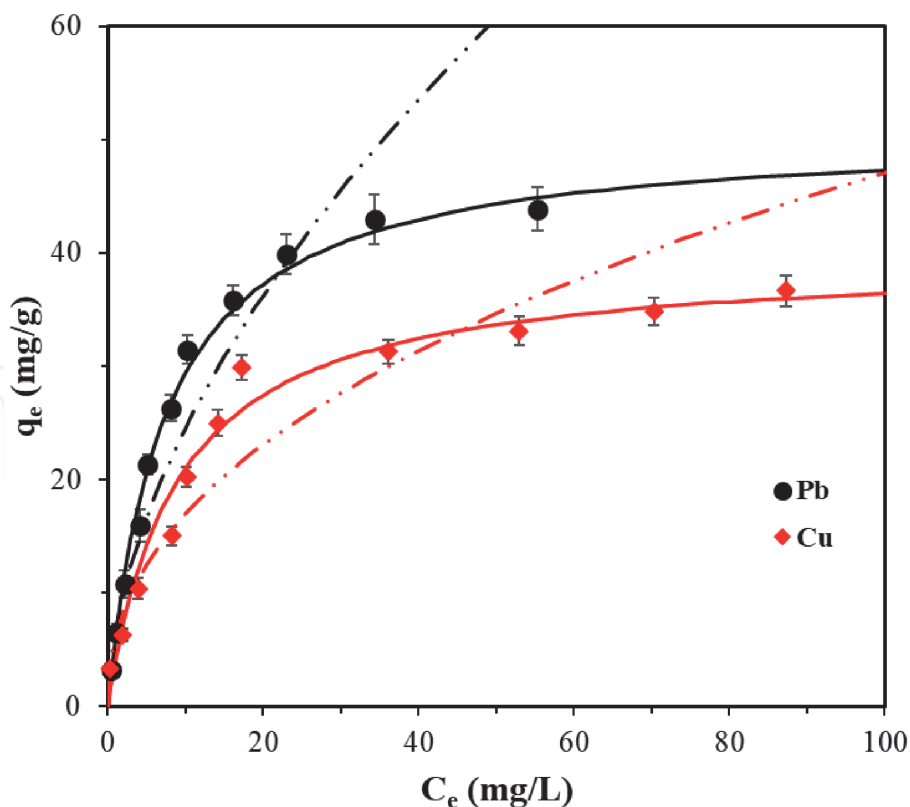


Figure 12. Equilibrium isotherms for Pb and Cu adsorption on BEC-ED (solid lines and dash-dotted represent Langmuir and Freundlich fitting, respectively).

stronger interactions with the lone pairs of electrons of the nitrogen atoms of amino groups than that of the Cu, as previously demonstrated elsewhere [63, 85]. Therefore, the Pb(II) ions can rapidly form a stable complex with $-NH_2$ groups on the surface of the BEC-ED.

The adsorption isotherm was modeled both by Freundlich (Eq. (6)) and Langmuir (Eq. (7)) models. The results revealed that the equilibrium isotherms data (**Figure 12** and **Table 7**) correlated better with the Langmuir model with a maximum adsorption capacity estimated at 50.76 mg/g and 39.68 mg/g for Pb(II) and Cu(II), respectively. This implies that the BEC-ED surface is homogeneous, which indicates that lead and copper ions adsorption follows monolayer adsorption.

To better understand the retention mechanisms of copper and lead adsorption on BEC-ED, the effect of lead and copper ions adsorption on the morphology of BEC-ED was monitored by SEM analysis. **Figure 13** shows the possible interactions between BEC-ED and the Pb(II) and Cu(II) ions, as well as the proposed mechanism. SEM pictures showed distortion in the morphology of BEC-ED under the adsorption forces of Pb(II) and Cu(II) ions. However, this effect is probably caused by the interactions between the metal ions and the donor sites of the grafted groups (ED), where the internal compression of the laminated structure has caused a very remarkable separation of the polymeric layers. Indeed, the approximate calculation

	Langmuir		Freundlich				
	q_{exp} (mg/g)	q_m (mg/g)	K_L (L/mg)	R^2	$1/n$	K_F (L/mg)	R^2
Pb	43.85	50.76	0.137	0.996	0.443	6.1	0.951
Cu	36.64	39.68	0.112	0.990	0.5636	6.7	0.944

Table 7. Freundlich and Langmuir constants for lead and copper adsorption on BEC-ED.

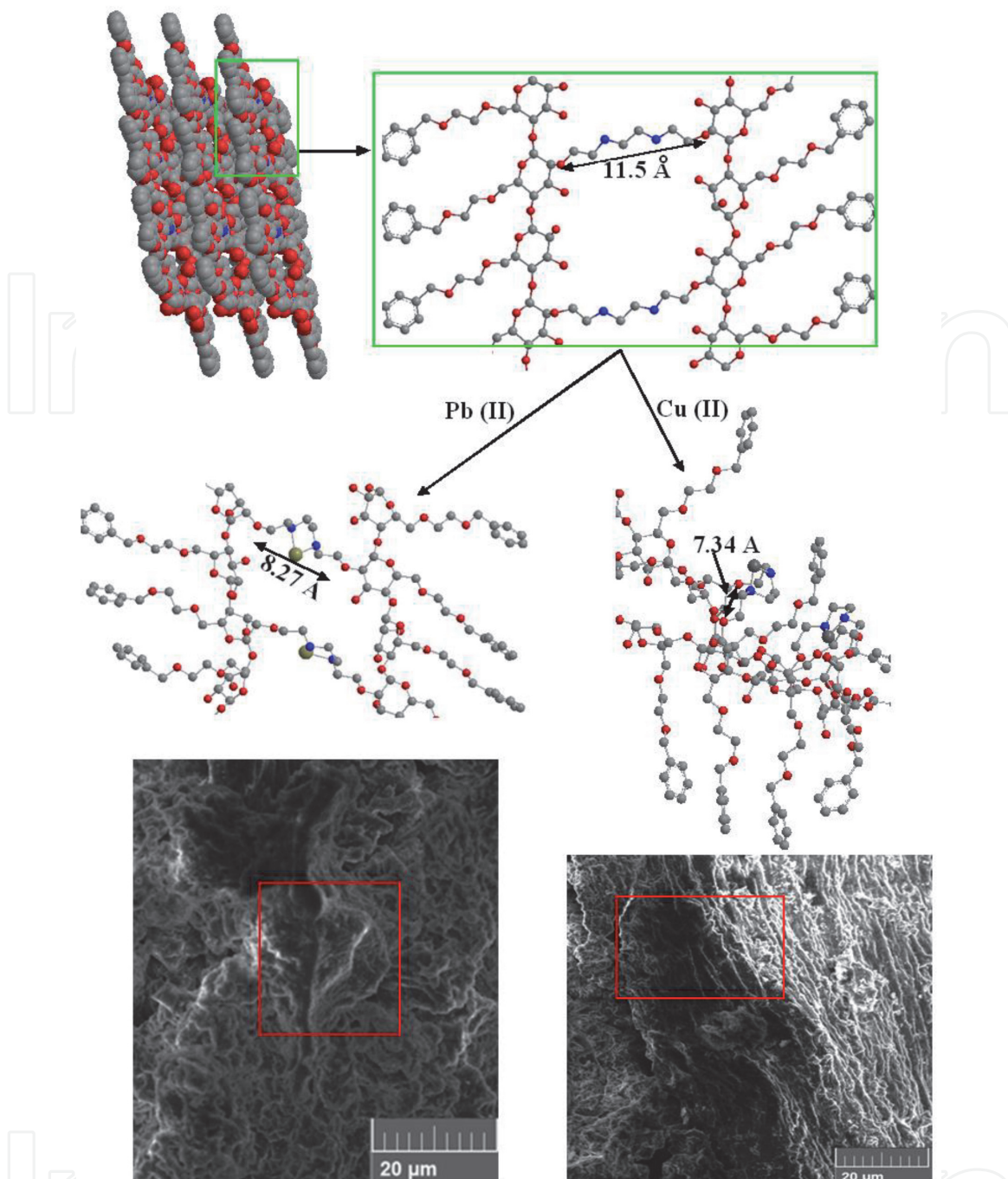


Figure 13.
Impact of the adsorption of lead and copper ions on the morphology of BEC-ED.

carried out to compare the inter-chain distances showed a decrease in the latter. The results obtained showed the capability of BEC-ED for adsorbing Cu(II) via metal interactions with NH_2 groups of ethylenediamine [56, 60], resulting in the decrease in the inter-layer distance from 11.50 Å to 07.34 Å for copper and 08.27 Å for lead.

For the purpose to assess the potential retention of lead and copper ions retention provided by BEC-ED compared to other adsorbents, the results achieved through this study were compared with the adsorption abilities of some conventional natural and synthetic cellulose in the literature (**Table 8**). It has been found that the lead and copper retention capacity of BEC-ED is among the higher results. Therefore, considering the retention capabilities of other adsorbents, accessibility, environment friendly biomaterial, and low cost, it may be concluded that the BEC-ED adsorbent demonstrated its ability to efficiently eliminate lead and copper ions in simple media.

Grafted cellulose adsorbent	Chelating group	Metal ions	Adsorption capacity (mg/g)	Ref.
Cellulose	Epichlorohydrin	Pb ²⁺ Cu ²⁺	38.02 72.99	[86]
Microcrystalline cellulose	Tetrafluoroterephthalonitrile	Pb ²⁺ Cu ²⁺	20.46 17.94	[87]
Cellulosic biopolymer	(alkali treatment)	Pb ²⁺ , Cd ²⁺ Zn ²⁺	67.24 44.42 16.85	[88]
CMC@ hydrogel	—	Cu ²⁺	2.30	[89]
BEC-ED	Ethylenediamine	Pb ²⁺ Cu ²⁺	50.76 39.68	this work this work

Table 8.

Comparison of lead and copper adsorption capacity of BEC-ED with conventional natural and synthetic cellulose adsorbents.

4. Conclusion

A new green adsorbent, Benzyloxyethyl cellulose crosslinked ED (BEC-ED) was successfully synthesized. The proposal structures were confirmed using vibrational spectroscopy, X-ray diffraction patterns, SEM images, x-ray EDS spectra, and TGA thermograms. The results showed that the ED crosslinking reaction of BEC engendered new structural significant modification at the crystalline and morphological levels. Ethylenediamine crosslinked BEC has been used for the removal of lead (Pb) and copper (Cu) from an aqueous system. The results revealed that the equilibrium isotherms data correlated better with the Langmuir model with a maximum adsorption capacity estimated at 50.76 mg/g and 39.68 mg/g for Pb (II) and Cu (II), respectively. In addition, the results demonstrated that the capability of BEC-ED for adsorbing Cu (II) and Pb (II) was governed by metal–ligand interactions with NH₂ chelator sites of ethylenediamine, resulting in the decrease in the civility diameter from 11.50 Å to 07.34 Å for copper and 08.27 Å for lead. However, these distortions proved the lamellar structure, and the separation of the sheets was observed on the SEM images of BEC-ED after adsorption.

Acknowledgements

We thank greatly the anonymous reviewers for their careful review and valuable suggestions on the manuscript. The authors are thankful to the Head of Oujda's chemistry department, Prof. Abdelmonaem TALHAOUI, for providing all the facilities and subsidies necessary to carry out the research work of this article. Our warm thanks are addressed to Prof. Gharibi EL KHADIR, Director of the Solid Mineral Solid Chemistry Laboratory – Oujda, for his sincere and persistent contributions and devoted cooperation.

Conflict of interest

The authors declared that there is no conflict of interest.

IntechOpen

Author details

Issam Jilal^{1*}, Soufian El Barkany^{1*}, Zahra Bahari¹, Youssef El Ouardi^{2,3},
Mohamed Loutou¹, Hassan Amhamdi⁴, Mohamed Abou-Salama¹, Amin Salhi⁴,
Abderrahmane El Idrissi⁵ and Katri Laatikainen³

1 Laboratory of Molecular Chemistry, Materials and Environment (LMCME),
Department of Chemistry, Faculty Multidisciplinary Nador, Mohamed 1st
University, Nador, Morocco

2 LIMOME Laboratory, Dhar El Mehraz Faculty of Sciences, Sidi Mohamed Ben
Abdellah University, Fes, Morocco


3 Laboratory of Separation Technology, Lappeenranta University of Technology,
Lappeenranta, Finland

4 Applied Chemistry Unit, Sciences and Technologies Faculty, Abdelmalek Essaadi
University, Al Hoceima, Morocco

5 Laboratory Applied Chemistry and Environmental (LCAE-URAC18), Faculty of
Sciences of Oujda, Mohamed1stUniversity, Oujda, Morocco

*Address all correspondence to: issamjilal@gmail.com
and el.barkany011@gmail.com

IntechOpen

© 2021 The Author(s). Licensee IntechOpen. This chapter is distributed under the terms of the Creative Commons Attribution License (<http://creativecommons.org/licenses/by/3.0>), which permits unrestricted use, distribution, and reproduction in any medium, provided the original work is properly cited. 

References

- [1] Hokkanen S, Bhatnagar A, Sillanpää M. A review on modification methods to cellulose-based adsorbents to improve adsorption capacity. *Water Research*. 2016;**91**:156-173. DOI: 10.1016/j.watres.2016.01.008
- [2] Pandiyan J, Mahboob S, Govindarajan M, Al-ghanim KA, Ahmed Z, Al-mulhm N, et al. An assessment of level of heavy metals pollution in the water, sediment and aquatic organisms: A perspective of tackling environmental threats for food security. *Saudi Journal of Biological Sciences*. 2021;**28**(2):1218-1225. DOI: 10.1016/j.sjbs.2020.11.072
- [3] Karimi A, Haghnia GH, Ayoubi S, Safari T. Impacts of geology and land use on magnetic susceptibility and selected heavy metals in surface soils of Mashhad plain, northeastern Iran. *Journal of Applied Geophysics*. 2017; **138**:127-134. DOI: 10.1016/j.jappgeo.2017.01.022
- [4] Kim HS, Kim YJ, Seo YR. An overview of carcinogenic heavy metal: molecular toxicity mechanism and prevention. *Journal of Cancer Prevention*. 2015;**20**(4):232. DOI: 10.15430/JCP.2015.20.4.232
- [5] Peng S, Dai M, Zhang J, Zhang M, Shi Q, Liang B, Zheng T. Dynamics of ecological risks associated with heavy metals in sediments during the construction process of the Yangtze River deepwater channel. *Journal of Cleaner Production*. 2020;**269**:122231. DOI: 10.1016/j.jclepro.2020.122231
- [6] Zhang J, Shi Q, Fan S, Zhang Y, Zhang M, Zhang J. Distinction between Cr and other heavy-metal-resistant bacteria involved in C/N cycling in contaminated soils of copper producing sites. *Journal of Hazardous Materials*. 2021;**402**:123454. DOI: 10.1016/j.jhazmat.2020.123454
- [7] Nriagu JO, Pacyna JM. Quantitative assessment of worldwide contamination of air, water and soils by trace metals. *Nature*. 1988;**333**(6169):134-139. DOI: 10.1038/333134a0
- [8] Ju X-J, Zhang S-B, Zhou M-Y, Xie R, Yang L, Chu L-Y. Novel heavy-metal adsorption material: ion-recognition P (NIPAM-co-BCAm) hydrogels for removal of lead (II) ions. *Journal of Hazardous Materials*. 2009;**167**(1-3): 114-118. DOI: 10.1016/j.jhazmat.2008.12.089
- [9] Priastomo Y, Setiawan HR, Kurniawan YS, Ohto K. Simultaneous removal of lead (II), chromium (III), and copper (II) heavy metal ions through an adsorption process using C-phenylcalix [4] pyrogallolarene material. *Journal of Environmental Chemical Engineering*. 2020;**8**(4): 103971. DOI: 10.1016/j.jece.2020.103971
- [10] Bankole MT, Abdulkareem AS, Mohammed IA, Ochigbo SS, Tijani JO, Abubakre OK, et al. Selected heavy metals removal from electroplating wastewater by purified and polyhydroxylbutyrate functionalized carbon nanotubes adsorbents. *Scientific Reports*. 2019;**9**(1):1-19. DOI: 10.1038/s41598-018-37899-4
- [11] Yatribi A, Nejmeddine A, Boukhars L. Contribution à la valorisation industrielle des déchets de tanneries: Cas de la cimenterie. In: *Annales de Chimie Science Des Matériaux*. Vol 26. Elsevier; 2001: 107-112.
- [12] Kushwaha A, Hans N, Kumar S, Rani R. A critical review on speciation, mobilization and toxicity of lead in soil-microbe-plant system and bioremediation strategies. *Ecotoxicology Environmental Safety*. 2018;**147**:1035-1045. DOI: 10.1016/j.ecoenv.2017.09.049

- [13] Mohan S, Sreelakshmi G. Fixed bed column study for heavy metal removal using phosphate treated rice husk. *Journal of Hazardous Materials*. 2008; **153**(1-2):75-82. DOI: 10.1016/j.jhazmat.2007.08.021
- [14] Zhang Y. 100 years of Pb deposition and transport in soils in Champaign, Illinois. USA. *Water Air and Soil Pollution*. 2003; **146**(1):197-210. DOI: 10.1023/A:1023957226204
- [15] Badawy NA, El-Bayaa AA, Abdel-Aal AY, Garamon SE. Chromatographic separations and recovery of lead ions from a synthetic binary mixtures of some heavy metal using cation exchange resin. *Journal of Hazardous Materials*. 2009; **166**(2-3):1266-1271. DOI: 10.1016/j.jhazmat.2008.12.044
- [16] Nordberg GF, Fowler BA. Nordberg M. *Handbook on the Toxicology of Metals*: Academic press; 2014
- [17] Jiang X, Liu W, Xu H, Cui X, Li J, Chen J, Zheng B. Characterizations of heavy metal contamination, microbial community, and resistance genes in a tailing of the largest copper mine in China. *Environmental Pollution*. Published online 2021:116947. DOI: 10.1016/j.envpol.2021.116947
- [18] Li L, Pan D, Li B, Wu Y, Wang H, Gu Y, et al. Patterns and challenges in the copper industry in China. *Resources, Conservation and Recycling*. 2017; **127**: 1-7. DOI: 10.1016/j.resconrec.2017.07.046
- [19] Chen Q, Yao Y, Li X, Lu J, Zhou J, Huang Z. Comparison of heavy metal removals from aqueous solutions by chemical precipitation and characteristics of precipitates. *Journal of water Process Engineering*. 2018; **26**: 289-300. DOI: 10.1016/j.jwpe.2018.11.003
- [20] Zhang Y, Duan X. Chemical precipitation of heavy metals from wastewater by using the synthetical magnesium hydroxy carbonate. *Water Science and Technology*. 2020; **81**(6): 1130-1136. DOI: 10.2166/wst.2020.208
- [21] Hube S, Eskafi M, Hrafnkelsdóttir KF, Bjarnadóttir B, Bjarnadóttir M, Axelsdóttir S, Wu B. Direct membrane filtration for wastewater treatment and resource recovery: A review. *Science of the Total Environment*. 2020; **710**:136375. DOI: 10.1016/j.scitotenv.2019.136375
- [22] Erçarıkçı E, Alanyalıoğlu M. Dual-Functional Graphene-Based Flexible Material for Membrane Filtration and Electrochemical Sensing of Heavy Metal Ions. *IEEE Sensors Journal*. 2020; **21**(3): 2468-2475. DOI: 10.1109/JSEN.2020.3021988
- [23] Sun Y, Zhou S, Pan S-Y, Zhu S, Yu Y, Zheng H. Performance evaluation and optimization of flocculation process for removing heavy metal. *Chemical Engineering Journal*. 2020; **385**:123911. DOI: 10.1016/j.cej.2019.123911
- [24] Swain K, Abbassi B, Kinsley C. Combined electrocoagulation and chemical coagulation in treating brewery wastewater. *Water*. 2020; **12**(3):726. DOI: 10.3390/w12030726
- [25] Yeh G, Hoang H-G, Lin C, Bui X, Tran H, Shern C, et al. Assessment of heavy metal contamination and adverse biological effects of an industrially affected river. *Environmental Science and Pollution Research*. 2020; **27**(28): 34770-34780. DOI: 10.1007/s11356-020-07737-0
- [26] Ibrahim Y, Naddeo V, Banat F, Hasan SW. Preparation of novel polyvinylidene fluoride (PVDF)-Tin (IV) oxide (SnO₂) ion exchange mixed matrix membranes for the removal of heavy metals from aqueous solutions. *Separation and Purification Technology*. 2020; **250**:117250. DOI: 10.1016/j.seppur.2020.117250

- [27] Bożęcka A, Orlof-Naturalna M, Sanak-Rydwlewska S. Removal of lead, cadmium and copper ions from aqueous solutions by using ion exchange resin C 160. *Gospod Surowcami Miner.* 2016;**32**. DOI: 10.1515/gospo-2016-0033
- [28] Dai K, Chen H, Peng T, Ke D, Yi H. Photocatalytic degradation of methyl orange in aqueous suspension of mesoporous titania nanoparticles. *Chemosphere.* 2007;**69**(9):1361-1367. DOI: 10.1016/j.chemosphere.2007.05.021
- [29] Zhao Y, Kang S, Qin L, Wang W, Zhang T, Song S, Komarneni S. Self-assembled gels of Fe-chitosan/montmorillonite nanosheets: dye degradation by the synergistic effect of adsorption and photo-Fenton reaction. *Chemical Engineering Journal.* 2020; 379:122322. DOI: 10.1016/j.cej.2019.122322
- [30] Saravanan R, Gupta VK, Narayanan V, Stephen A. Comparative study on photocatalytic activity of ZnO prepared by different methods. *Journal of Molecular Liquids.* 2013;**181**:133-141. DOI: 10.1016/j.molliq.2013.02.023Get
- [31] Saravanan R, Khan MM, Gupta VK, Mosquera E, Gracia F, Narayanan V, et al. ZnO/Ag/Mn₂O₃ nanocomposite for visible light-induced industrial textile effluent degradation, uric acid and ascorbic acid sensing and antimicrobial activity. *RSC Advances.* 2015;**5**(44):34645-34651. DOI: 10.1039/C5RA02557E
- [32] Qi Y, Zhu L, Shen X, Sotto A, Gao C, Shen J. Polyethyleneimine-modified original positive charged nanofiltration membrane: Removal of heavy metal ions and dyes. *Separation and Purification Technology.* 2019;**222**: 117-124. DOI: 10.1016/j.seppur.2019.03.083
- [33] Jilal I, El Barkany S, Bahari Z, Sundman O, El Idrissi A, Abou-Salama M, et al. New quaternized cellulose based on hydroxyethyl cellulose (HEC) grafted EDTA: synthesis, characterization and application for Pb (II) and Cu (II) removal. *Carbohydrate Polymers.* 2018;**180**:156-167. DOI: 10.1016/j.carbpol.2017.10.012
- [34] Liu Q, Li Y, Chen H, Lu J, Yu G, Moslang M, Zhou Y. Superior adsorption capacity of functionalised straw adsorbent for dyes and heavy-metal ions. *Journal of Hazardous Materials.* 2020;**382**:121040. DOI: 10.1016/j.jhazmat.2019.121040
- [35] Choi HY, Bae JH, Hasegawa Y, An S, Kim I, Lee H, Kim M. Thiol-functionalized cellulose nanofiber membranes for the effective adsorption of heavy metal ions in water. *Carbohydrate Polymers.* 2020;**234**: 115881. DOI: 10.1016/j.carbpol.2020.115881
- [36] Jiang C, Wang X, Hou B, Hao C, Li X, Wu J. Construction of a lignosulfonate-lysine hydrogel for the adsorption of heavy metal ions. *Journal Agricultural and Food Chemistry.* 2020;**68**(10):3050-3060. DOI: 10.1021/acs.jafc.9b07540
- [37] Niu M, Li G, Cao L, Wang X, Wang W. Preparation of sulphate aluminate cement amended bentonite and its use in heavy metal adsorption. *Journal of Cleaner Production.* 2020;**256**: 120700. DOI: 10.1016/j.jclepro.2020.120700
- [38] Yap PL, Auyoong YL, Hassan K, Farivar F, Tran D, Ma J, Losic D. Multithiol functionalized graphene bio-sponge via photoinitiated thiol-ene click chemistry for efficient heavy metal ions adsorption. *Chemical Engineering Journal.* 2020;**395**:124965. DOI: 10.1016/j.cej.2020.124965
- [39] Lacuesta AC, Herrera MU, Manalo R, Balela MDL. Fabrication of kapok paper-zinc oxide-polyaniline

hybrid nanocomposite for methyl orange removal. *Surface and Coatings Technology*. 2018;**350**:971-976. DOI: 10.1016/j.surfcoat.2018.03.043

[40] Herrera MU, Futralan CM, Gapusan R, Balela MDL. Removal of methyl orange dye and copper (II) ions from aqueous solution using polyaniline-coated kapok (*Ceiba pentandra*) fibers. *Water Science and Technology*. 2018;**78**(5):1137-1147. DOI: 10.2166/wst.2018.385

[41] Balela MDL, Intila NM, Salvanera SR. Adsorptive Removal of Lead Ions in Aqueous Solution by Kapok-Polyacrylonitrile Nanocomposites. *Materials Today Proceeding*. 2019;**17**:672-678. DOI: 10.1016/j.matpr.2019.06.349

[42] Awual MR, Yaita T, Okamoto Y. A novel ligand based dual conjugate adsorbent for cobalt (II) and copper (II) ions capturing from water. *Sensors and Actuators B Chemical*. 2014;**203**:71-80. DOI: 10.1016/j.snb.2014.06.088

[43] El Ouardi Y, Branger C, Toufik H, Laatikainen K, Ouammou A, Lenoble V. An insight of enhanced natural material (calcined diatomite) efficiency in nickel and silver retention: Application to natural effluents. *Environmental Technology and Innovation*. 2020;**18**:100768. DOI: 10.1016/j.eti.2020.100768

[44] El-Saied H, Mostafa AM, Hasanin MS, Mwafy EA, Mohammed AA. Synthesis of antimicrobial cellulosic derivative and its catalytic activity. *Journal of King Saud University-Science*. 2020;**32**(1): 436-442. DOI: 10.1016/j.jksus.2018.06.007

[45] Abou-Yousef H, Dacrory S, Hasanin M, Saber E, Kamel S. Biocompatible hydrogel based on aldehyde-functionalized cellulose and chitosan for potential control drug release. *Sustainable Chemistry and*

Pharmacy. 2021;**21**:100419. DOI: 10.1016/j.scp.2021.100419

[46] Salama A. Cellulose/silk fibroin assisted calcium phosphate growth: Novel biocomposite for dye adsorption. *International Journal of Biological Macromolecules*. 2020;**165**:1970-1977. DOI: 10.1016/j.ijbiomac.2020.10.074

[47] Salama A. New sustainable hybrid material as adsorbent for dye removal from aqueous solutions. *Journal of Colloid and Interface Science*. 2017;**487**: 348-353. DOI: 10.1016/j.jcis.2016.10.034

[48] Dacrory S, Hashem AH, Hasanin M. Antifungal activity and hemocompatibility of cellulose based amino acid functionalized nano-biocomplex. *Environmental Nanotechnology, Monitoring & Management*. Published online 2021: 100453. DOI: 10.1016/j.enmm.2021.100453

[49] Putro JN, Santoso SP, Ismadji S, Ju Y-H. Investigation of heavy metal adsorption in binary system by nanocrystalline cellulose-bentonite nanocomposite: improvement on extended Langmuir isotherm model. *Microporous and Mesoporous Materials*. 2017;**246**:166-177. DOI: 10.1016/j.micromeso.2017.03.032

[50] Chen Q, Zheng J, Wen L, Yang C, Zhang L. A multi-functional-group modified cellulose for enhanced heavy metal cadmium adsorption: Performance and quantum chemical mechanism. *Chemosphere*. 2019;**224**: 509-518. DOI: 10.1016/j.chemosphere.2019.02.138

[51] Godiya CB, Cheng X, Li D, Chen Z, Lu X. Carboxymethyl cellulose/polyacrylamide composite hydrogel for cascaded treatment/reuse of heavy metal ions in wastewater. *Journal of Hazardous Materials*. 2019;**364**:28-38. DOI: 10.1016/j.jhazmat.2018.09.076

- [52] Dacrory S, Abou-Yousef H, Kamel S, Turky G. Development of biodegradable semiconducting foam based on micro-fibrillated cellulose/Cu-NPs. *International Journal of Biological Macromolecules*. 2019;**132**:351-359. DOI: 10.1016/j.ijbiomac.2019.03.156
- [53] El Barkany S, El Idrissi A, Zanagui C, Jilal I, Tabghat F, Abou-Salama M, et al. New branched chain cellulose derivatives based on esparto *Stipa tenacissima* of eastern Morocco: synthesis and characterization. *Journal of Materials Environment Science*. 2017; **8**(4):1195-1210
- [54] Jilal I, El Barkany S, Bahari Z, Sundman O, El Idrissi A, Salhi A, et al. Unconventional synthesis, characterization and theoretical study (HF and DFT computations) of new cellulosic copper complex: benzyloxyethyl cellulose copper (CuBEC). *Cellulose*. 2018;**25**(8): 4375-4388. DOI: 10.1007/s10570-018-1909-x
- [55] Chaouf S, El Barkany S, Amhamdi H, Jilal I, El Ouardi Y, Abou-Salama M, et al. Low degree of substitution of cellulose acrylate based green polyelectrolyte: Synthesis, characterization and application to the removal of Cu (II) ions and colloidal Fe (OH) 3 turbidity. *Materials Today Proceeding*. 2020;**31**:S175-S182. DOI: 10.1016/j.matpr.2020.07.512
- [56] Yakout AA, El-Sokkary RH, Shreadah MA, Hamid OGA. Cross-linked graphene oxide sheets via modified extracted cellulose with high metal adsorption. *Carbohydrate Polymers*. 2017;**172**:20-27. DOI: 10.1016/j.carbpol.2017.05.004
- [57] Guo Z, Fan J, Zhang J, Kang Y, Liu H, Jiang L, et al. Sorption heavy metal ions by activated carbons with well-developed microporosity and amino groups derived from *Phragmites australis* by ammonium phosphates activation. *Journal of the Taiwan Institute of Chemical Engineers*. 2016; **58**:290-296. DOI: 10.1016/j.jtice.2015.05.041
- [58] Wu F-C, Tseng R-L, Juang R-S. Kinetic modeling of liquid-phase adsorption of reactive dyes and metal ions on chitosan. *Water Research*. 2001; **35**(3):613-618. DOI: 10.1016/S0043-1354(00)00307-9
- [59] Yoshitake H, Yokoi T, Tatsumi T. Adsorption behavior of arsenate at transition metal cations captured by amino-functionalized mesoporous silicas. *Chemistry of Materials*. 2003; **15**(8):1713-1721. DOI: 10.1021/cm0218007
- [60] Racho P, Phalathip P. Modified nylon fibers with amino chelating groups for heavy metal removal. *Energy Procedia*. 2017;**118**:195-200. DOI: 10.1016/j.egypro.2017.07.026
- [61] Liang X, Liang B, Wei J, Zhong S, Zhang R, Yin Y, et al. A cellulose-based adsorbent with pendant groups of quaternary ammonium and amino for enhanced capture of aqueous Cr (VI). *International Journal of Biological Macromolecules*. 2020;**148**:802-810. DOI: 10.1016/j.ijbiomac.2020.01.184
- [62] Wang J, Zhao L, Duan W, Han L, Chen Y. Adsorption of aqueous Cr (VI) by novel fibrous adsorbent with amino and quaternary ammonium groups. *Industrial & Engineering Chemistry Research*. 2012;**51**(42):13655-13662. DOI: 10.1021/ie3013874
- [63] Wang K, Gu J, Yin N. Efficient removal of Pb (II) and Cd (II) using NH₂-functionalized Zr-MOFs via rapid microwave-promoted synthesis. *Industrial & Engineering Chemistry Research*. 2017;**56**(7):1880-1887. DOI: 10.1021/acs.iecr.6b04997
- [64] Edebali S, Pehlivan E. Evaluation of chelate and cation exchange resins to

remove copper ions. Powder Technology. 2016;**301**:520-525. DOI: 10.1016/j.powtec.2016.06.011

[65] Gupta S, Varshney PK. Effect of plasticizer concentration on structural and electrical properties of hydroxyethyl cellulose (HEC)-based polymer electrolyte. Ionics (Kiel). 2017; **23**(6):1613-1617. DOI: 10.1007/s11581-017-2116-8

[66] Fiayaz M, Zia KM, Javaid MA, Rehman S, Chatha SAS, Zuber M. Synthesis and characterization of hydroxyethyl cellulose (HEC)-TiO₂-based polyurethane bionanocomposites. Korean Journal of Chemical Engineering. 2020;**37**(12):2351-2358. DOI: 10.1007/s11814-020-0664-5

[67] El Idrissi A, El Barkany S, Amhamdi H, Maaroufi A. Synthesis and characterization of the new cellulose derivative films based on the hydroxyethyl cellulose prepared from esparto "stipa tenacissima" cellulose of Eastern Morocco. II. Esterification with acyl chlorides in a homogeneous medium. Journal of Applied Polymer Science. 2013;**127**(5):3633-3644. DOI: 10.1002/app.37982

[68] Nizan NSNH, Zulkifli FH. Reinforcement of hydroxyethyl cellulose/poly (vinyl alcohol) with cellulose nanocrystal as a bone tissue engineering scaffold. Journal of Polymer Research. 2020;**27**:1-9. DOI: 10.1007/s10965-020-02112-6

[69] Das A, Kundu S, Ghosh SK, Basu A, Gupta M, Mukherjee A. Guar gum cinnamate ouzo nanoparticles for bacterial contact killing in water environment. Carbohydrate Research. 2020;**491**:107983. DOI: 10.1016/j.carres.2020.107983

[70] Jafari M, Davachi SM, Mohammadi-Rovshandeh J, Pouresmael-Selakjani P. Preparation and characterization of bionanocomposites based on benzylated

wheat straw and nanoclay. Journal of Polymers Environmental. 2018;**26**(3): 913-925. DOI: 10.1007/s10924-017-0997-2

[71] Kundu S, Das A, Basu A, Abdullah MF, Mukherjee A. Guar gum benzoate nanoparticle reinforced gelatin films for enhanced thermal insulation, mechanical and antimicrobial properties. Carbohydrate Polymers. 2017;**170**:89-98. DOI: 10.1016/j.carbpol.2017.04.056

[72] Li M-F, Sun S-N, Xu F, Sun R-C. Cold NaOH/urea aqueous dissolved cellulose for benzylation: Synthesis and characterization. European Polymer Journal. 2011;**47**(9):1817-1826. DOI: 10.1016/j.eurpolymj.2011.06.013

[73] da Silva Filho EC, de Melo JCP, Airoidi C. Preparation of ethylenediamine-anchored cellulose and determination of thermochemical data for the interaction between cations and basic centers at the solid/liquid interface. Carbohydrate Research. 2006; **341**(17):2842-2850. DOI: 10.1016/j.carres.2006.09.004

[74] de Melo JCP, da Silva Filho EC, Santana SAA, Airoidi C. Maleic anhydride incorporated onto cellulose and thermodynamics of cation-exchange process at the solid/liquid interface. Colloids Surfaces A: Physicochemical Engineering Aspects. 2009;**346**(1-3):138-145. DOI: 10.1016/j.colsurfa.2009.06.006

[75] Pavia DL, Lampman GM, Kriz GS, Vyvyan JA. Introduction to Spectroscopy. Nelson Education. 2014

[76] Da Silva Filho EC, de Barros Júnior JF, Santana SAA, de Melo JCP, Airoidi C. Thermodynamics of cation/basic center interactions from ethylene-1, 2-diamine? pentane-2, 4-dione cellulose incorporated. Glob. J Phys Chem. 2011;**2**:277-286

- [77] El Ghali A, Baouab MHV, Roudesli MS. Preparation, characterization and application of a [copper (II)/ethylenediamine–cotton] complex for the removal of AB25 from aqueous solution in a laboratory scale column. *Chemical Engineering Journal*. 2011;**174**(1):18-26. DOI: 10.1016/j.cej.2011.07.046
- [78] Dhahri A, Beyou E, Alcouffe P, Serghei A, Baouab MHV. Synthesis and characterization of Au-immobilized nanoparticles onto cellulose-ethylenediamine-grafted reduced graphite oxide sheets. *Materials Chemistry and Physics*. 2016;**171**: 303-311. DOI: 10.1016/j.matchemphys.2016.01.021
- [79] Ramírez JAÁ, Hoyos CG, Arroyo S, Cerrutti P, Foresti ML. Acetylation of bacterial cellulose catalyzed by citric acid: Use of reaction conditions for tailoring the esterification extent. *Carbohydrate Polymers*. 2016;**153**: 686-695. DOI: 10.1016/j.carbpol.2016.08.009
- [80] Jung KW, Kim DH, Kim HW, Shin HS. Optimization of combined (acid + thermal) pretreatment for fermentative hydrogen production from *Laminaria japonica* using response surface methodology (RSM). *International Journal of Hydrogen Energy*. 2011;**36**(16):9626-9631. DOI: 10.1016/j.ijhydene.2011.05.050
- [81] Ignasi Puigdomenech. *Hydra/ Medusa Chemical Equilibrium Database and Plotting Software* (2015).
- [82] El Ouardi Y, Branger C, Laatikainen K, Durrieu G, Mounier S, Ouammou A, et al. Impact of thermal treatment on bentonite retention ability toward nickel and silver retention. *Separation Science and Technology*. 2020;**55**(18):1-18)11. DOI: 10.1080/01496395.2020.1839772
- [83] Freundlich H. Über die Adsorption in Lösungen. *Zeitschrift für Physikalische Chemie*. 1906;**57**(4): 385-470
- [84] Langmuir I. The adsorption of gases on plane surfaces of glass, mica and platinum. *Journal of the American Chemical Society*. 1918;**345**(1914): 1361-1403. DOI: 10.1021/ja02242a004
- [85] Ahmadijokani F, Tajahmadi S, Bahi A, Molavi H, Rezakaezmi M, Ko F, et al. Ethylenediamine-functionalized Zr-based MOF for efficient removal of heavy metal ions from water. *Chemosphere*. 2021;**264**. DOI: 10.1016/j.chemosphere.2020.128466
- [86] Taksitta K, Sujarit P, Ratanawimarnwong N, Donpuksa S, Songsrirote K. Development of tannin-immobilized cellulose fiber extracted from coconut husk and the application as a biosorbent to remove heavy metal ions. *Environmental Nanotechnology, Monitoring & Management*. 2020;**14** (October):100389. DOI: 10.1016/j.enmm.2020.100389
- [87] Cao J, Fei D, Tian X, Zhu Y, Wang S, Zhang Y, et al. Novel modified microcrystalline cellulose-based porous material for fast and effective heavy-metal removal from aqueous solution. *Cellulose*. 2017;**24**(12):5565-5577. DOI: 10.1007/s10570-017-1504-6
- [88] Singha AS, Guleria A. Use of Low Cost Cellulosic Biopolymer Based Adsorbent for the Removal of Toxic Metal Ions from the Aqueous Solution. *Separation Science and Technology*. 2014;**49**(16):2557-2567. DOI: 10.1080/01496395.2014.929146
- [89] Baiya C, Nannuan L, Tassanapukdee Y, Chailapakul O, Songsrirote K. The Synthesis of Carboxymethyl Cellulose-Based Hydrogel from Sugarcane Bagasse Using Microwave-Assisted Irradiation for Selective Adsorption of Copper(II) Ions. *Environmental Progress & Sustainable Energy*. 2019;**38**(s1):S157-S165. DOI: 10.1002/ep.12950